COMPOSITION OF MESSENGER SURFACE TYPES FROM MULTRISPECTRAL MASCS DATA. K. R. Stockstill-Cahill[1], J. T. S. Cahill[2], D. Domingue[1], N. R. Izenberg[2], and M. D'Amore[3], [1]Planetary Science Institute, (1700 East Fort Lowell, Suite 106, Tucson, AZ 85719-2395), [2]JHU/Applied Physics Laboratory (11100 Johns Hopkins Road, Laurel MD, 20723), [3](Inst. for Planetary Research, DLR, Rutherfordstrasse 2, 12489 Berlin, Germany).

Introduction: Orbital data from the Mercury Surface, Space ENvironment, GEochemestry, and Ranging (MESSENGER) mission allowed distinct geochemical regions to be defined [1,2] using the X-ray Spectrometer (XRS) and Gamma-Ray and Neutron Spectrometer (GRNS) data. Normative analyses of the elemental composition data for nine distinct geochemical regions were used to constrain the mineralogy present at Mercury's surface [2]. That work yielded mineralogies dominated by silicates (plagioclase, pyroxene, olivine, quartz). In addition, global maps of space weathering products for Mercury, including both nanophase and microphase Fe and C, were produced using radiative transfer models of MESSENGER's VIsisble and Infrared Spectrograph (VIRS) data [3]. Using these two results, we used the radiative transfer model of Hapke [4-6] to predict bidirectional reflectance spectra in a forward modeling approach [7,8].

In Hapke's model, the reflectance spectrum of a regolith is computed linearly from the single-scattering albedos (SSA) of mineral end-members [5,6]. The SSA is the probability that a photon incident on a regolith particle will be scattered rather than absorbed. It is independent of illumination or viewing geometry and a function of a grain's scattering behavior and absorption coefficient. The absorption coefficient is governed by the material's complex index of refraction, which is a function of the optical constants. Optical constants are wavelength-dependent quantities unique to each particle type in a regolith and represent the inherent physical and chemical properties of each material [9].

In order to accurately interpret reflectance spectra for airless bodies, the effects of opaque phases (e.g., Fe, Ni, sulfides) must be considered properly. Opaque metals are present as native igneous minerals in meteorites and on planetary surfaces in the form of grains that are significantly larger than the wavelength of the incident light. However, nanophase metal grains are a key by-product of space weathering [6,10-12] and introduce confounding effects on ultraviolet (UV), visible (VIS), and near-infrared (NIR) spectra as seen in laboratory and spacecraft data for airless bodies.

To address this issue, our model also included optical constants for opaque metal and mineral phases. Metals are present in planetary regolith in three spectrally-significant grain size categories: macroscopic, microphase, and nanophase [6, 13-18]. Macroscopic metal particles are large relative to the wavelength of light and grains of this size are often found as native igneous species in meteorites and lunar samples [19]. Microphase particles (e.g., $mpFe^0$) have diameters from ~50 nm to ~3000 nm, produce an overall decrease in reflectance with few effects on the continuum slope of a spectrum [12, 17, 18]. Finer-grained metal (<50 nm in diameter) is referred to as "nanophase metal" (e.g., $npFe^0$) and decreases the overall reflectance and introduces a strong positive spectral slope across the visible to NIR (i.e., spectral "reddening") [11, 12].

Methods: The model used was adapted from the work of [17], which uses optical constants for metals (Fe, Ni) to introduce the darkening and/or reddening effects of microscopic and nanophase metal on a reflectance spectrum. Required inputs are the abundance and composition of phases (including plagioclase, ilmenite, olivine, orthopyroxene, clinopyroxene, glass, agglutinates, macrometal, nanophase metal, microphase metal) as well as the grain sizes of the (macrophase) host particles and the microphase metal.

We have adapted the algorithm for applications to other airless planetary bodies, including Mercury. For this study, we sought to extend the opaque phases available for spectral mixing and space weathering, which were previously centered on the Fe-rich nature of the Moon (e.g., metallic Fe). Results of these models relative to MESSENGER spectra will be presented.

Example - Rachmaninoff Basin: In this abstract, we present example results for the Rachmaninoff Basin region (Fig. 1). The Rachmaninoff Basin region (centered at ~28°N, ~303°E) is the most prominent region of high Mg/Si outside of the high Mg region [1], with the area with the highest Mg/Si found within the peak ring and NW portions of the annular ring (Fig. 2). The peak ring contains relatively young volcanic smooth plains and differs markedly in albedo from the plains in the surrounding annular ring [20], which match the spectral properties of the low-reflectance material (LRM) [21]. Weider et al. [1] suggested that this impact excavated an Mg-rich magmatic body with sulfides representing the darkening agent.

The CIPW normative results for Rachmaninoff Basin suggest that it is dominated by plagioclase and olivine, with lesser amounts of pyroxene (Table 1). When using a high-Mg classification scheme, Vander Kaaden et al. [2] found that it spanned the boundary between komatiites and boninites. The dominant space weathering products found within the basin are microphase Fe and nanophase carbon (Table 1). These abundances guided the input values for this study.

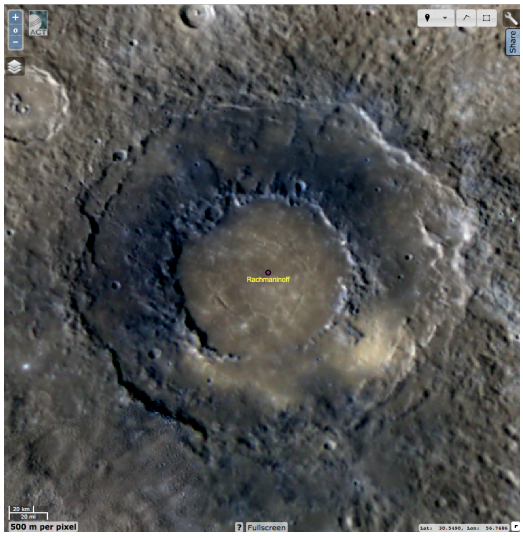

Figure 1: A quick map view of Rachmaninoff Basin using the 8-Color Global MDIS map, showing the albedo variation present in the annular rings.

Table 1: Mineral & space weathering product abundances from [2,3] and from this study.

	RB [2]		Model
Plagioclase	41.99%	**Plagioclase**	42.0%
Olivine	24.17%	**Olivine**[1]	24.2%
Diopside	16.04%	**Cpx**[1,2]	16.0%
Hypersthene	11.45%	**Opx**[1,3]	12.4%
Sulfides	5.42%	**Sulfides**	5.4%
Opx	0.95%		
Sum	100.02%	**Sum**	100%
	RB [3]		**Model**
micro Fe	1.75%	**micro Fe**	1.75%
nano C	1.5%	**nano C**	1.5%

[1]Mg#=90; [2]Clinopyroxene; [3]Orthopyroxene (includes hypersthene and Opx from [2]).

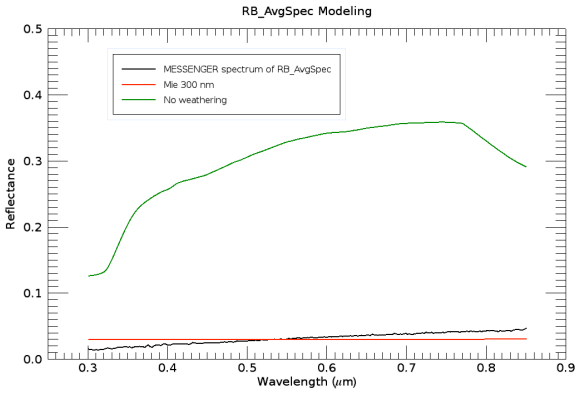

Figure 3: Model spectra (red and green) compared to MASCS spectrum of Rachmaninoff Basin. Red spectrum included 300 nm microphase Fe grains and nanophase carbon; the green spectrum contains no space weathering products.

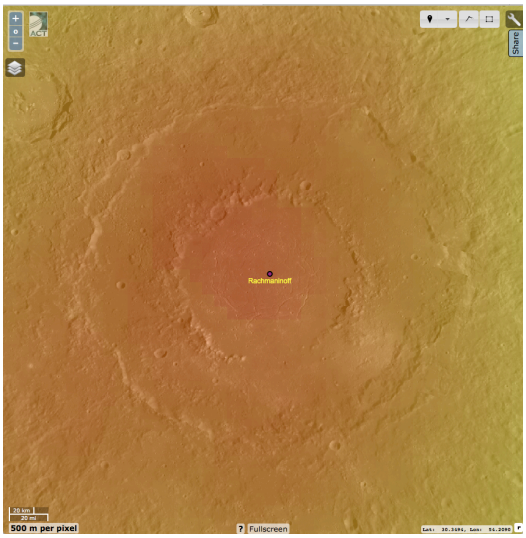

Figure 2: Quick map view of Mg/Si of the Rachmaninoff Basin region [1].

Results: Initial modeling results for Rachmaninoff Basin using the mineralogy and space weathering products derived by [2,3] are shown in Figure 3. The spectrum with no space weathering (green) does not match the albedo or shape of the MASCS spectrum (black). When microphase Fe and nanophase carbon are included in the model, the spectrum (red) matches the overall albedo for the weathered spectrum, but fails to match the overall slope. Systematic variations to the model variables (grain sizes, Mg#, An for plag) will be implemented to improve the model fits for Rachmaninoff and other geochemical regions.

References: [1] Weider, S. Z. et al. (2015) *EPSL*, 416, 109-120. [2] Vander Kaaden et al. (2016) *Icarus, in press*. [3] Trang D. et al. (2017) *Icarus, in prep*. [4] Hapke, B. (1981), *JGR, 86(B4)*, 3039–3054. [5] Hapke, B. (1993), *Theory of Reflectance and Emittance Spectroscopy*, Cambridge Univ. Press, U.K. [6] Hapke, B. (2001), *JGR, 106*, 10,039–10,073. [7] Lucey (1998) *JGR*, *103*, 3679–3699. [8] Wilcox et al. (2006), *JGR*, *111*. [9] Palik (1991), *Handbook of Optical Constants v.2*, Academic Press, Boston. [10] Keller and McKay (1997), *GCA, 61*, 2331–2341. [11] Pieters et al. (2000), *Meteorit. & Planet. Sci., 35*, 1101–1107. [12] Noble, et al. (2007) *Icarus*, 192, 629–642. [13] Britt and Pieters (1994), *GCA, 58*, 3905–3919. [14] Pieters et al. (2000) *Meteorit. Planet. Sci*., *35*, 1101–1107. [15] Noble and Pieters (2003), *JGR, 111*. [16] Nobel et al. (2006) *JGR*, *111*. [17] Lucey and Noble (2008) *Icarus*, *197(1)*, 348–353. [18] Lucey and Riner (2011) *Icarus*, *212*, 451–462. [19] Lawrence and Lucey (2007) *JGR, 112*. [20] Cahill et al. (2015) *JGR, 115*. [20] Prockter et al. (2010) *Science*, 329, 668-671. [21] Denevi et al. (2009) *JGR*, 118, 891-907.